Published in final edited form as:

Nat Struct Mol Biol. 2008 July ; 15(7): 754–760. doi:10.1038/nsmb.1442.

GroEL as a molecular scaffold for structural analysis of the anthrax toxin pore

Hiroo Katayama[1,5], **Blythe E Janowiak**[2,5], **Marek Brzozowski**[1], **Jordan Juryck**[1], **Scott Falke**[3], **Edward P Gogol**[4], **R John Collier**[2], and **Mark T Fisher**[1]

[1]Department of Biochemistry and Molecular Biology, University of Kansas Medical Center, 3901 Rainbow Blvd., Kansas Life Sciences Innovation Center Building, Kansas City, Kansas 66160, USA

[2]Department of Microbiology and Molecular Genetics, Harvard Medical School, Alpert Building, Boston, Massachusetts 02115, USA

[3]Department of Biology, William Jewell College, 500 College Hill, Liberty, Missouri 64068-1896, USA

[4]School of Biological Sciences, University of Missouri-Kansas City, Kansas City, Missouri 64100, USA

Abstract

We analyzed the 440-kDa transmembrane pore formed by the protective antigen (PA) moiety of anthrax toxin in the presence of GroEL by negative-stain electron microscopy. GroEL binds both the heptameric PA prepore and the PA pore. The latter interaction retards aggregation of the pore, prolonging its insertion-competent state. Two populations of unaggregated pores were visible: GroEL-bound pores and unbound pores. This allowed two virtually identical structures to be reconstructed, at 25-Å and 28-Å resolution, respectively. The structures were mushroom-shaped objects with a 125-Å-diameter cap and a 100-Å-long stem, consistent with earlier biochemical data. Thus, GroEL provides a platform for obtaining initial glimpses of a membrane protein structure in the absence of lipids or detergents and can function as a scaffold for higher-resolution structural analysis of the PA pore.

Correspondence should be addressed to M.T.F. (mfisher1@kumc.edu).
[5]These authors contributed equally to this work.

AUTHOR CONTRIBUTIONS

H.K. and B.E.J. contributed equally to the experimental design, the execution of the experiments and the interpretation of the data; they also contributed to the writing of the manuscript. Undergraduates J.J. and M.B. were involved in computer setup, network support, image scanning, data cataloging, some particle picking and initial alignment work under the guidance of H.K., S.F., E.P.G. and M.T.F. E.P.G, R.J.C. and M.T.F. contributed to experimental design, provided guidance, analysis and interpretation of the data and were responsible for writing the manuscript.

COMPETING INTERESTS STATEMENT

The authors declare competing financial interests: details accompany the full-text HTML version of the paper at http://www.nature.com/nsmb/.

Anthrax toxin has attracted considerable attention in recent years, primarily because of its relevance to the pathogenesis of *Bacillus anthracis*, a bioterrorism agent. Less widely appreciated is the fact that this toxin also provides a simple and tractable system for studying how a large globular protein can be translocated across a membrane. In the latter context, effort has been focused on understanding how the pore-forming heptameric component of the toxin, termed protective antigen (83 kDa), transports the two enzymatic moieties—lethal factor (LF; 90 kDa), a protease, and edema factor (89 kDa), an adenylyl cyclase—across the endosomal membrane of mammalian cells.

Anthrax toxin action begins when monomeric PA binds to a cellular receptor and is activated by a member of the furin family of cellular proteases (reviewed in ref. 1). The resulting 63-kDa activated form spontaneously oligomerizes to generate a ring-shaped heptamer, termed the PA prepore. The PA prepore in turn binds one or both of the enzymatic toxin components1, and the resulting complexes are endocytosed and trafficked to the endosomal compartment. There, under the influence of the acidic pH, the prepore undergoes a conformational rearrangement that allows it to form a PA pore in the membrane. The enzymatic moieties are then translocated in unfolded form through the pore to the cytosol, where they refold and modify their substrates, eliciting the toxic responses associated with anthrax infections. This unidirectional transport is driven primarily by a pH gradient and has been suggested to proceed by a brownian ratchet charge-state mechanism2.

The PA prepore can be isolated free in solution by column chromatography of trypsin-activated PA, and when exposed to mildly acidic conditions, it forms channels in model membranes that seem to be functionally similar, if not identical, to those formed in the endosomal membrane. However, the ability of the PA heptamer pore to insert into membranes is transient, as the complex rapidly becomes insoluble under acidic conditions and forms amorphous aggregates. Attempts to obtain crystals of the PA pore have met with failure, and thus far there has not been a published report of electron microscopic analysis of its structure.

Membrane protein structures are notoriously difficult to study, largely because of solubility constraints. Therefore, investigators must first find the proper conditions for solubilization, usually by testing a battery of different detergent and lipid formulations, before beginning structural analysis. Notably, membrane proteins bacteriorhodopsin and LacY and the bacteriophage λ holin can be sequestered in the substrate-binding cavity of the chaperonin GroEL in their membrane-insertable states in the absence of lipids or detergents3,4. Given these findings, and because it shares the seven-fold symmetry of the PA heptamer, we hypothesized that GroEL might bind to and stabilize the PA pore.

Biochemical studies5,6 and the X-ray crystallographic structure of the PA prepore7,8 suggest that the PA pore is a mushroom-shaped object with a globular cap and a long, 14-strand β-barrel stem (~100 Å) resembling that of the staphylococcal α-hemolysin9,10. The putative β-barrel forms after the massive unfolding of a substantial portion of domain 2 of the soluble prepore. At the end of the β-barrel is a region that contains a critical hydrophobic loop that inserts into the membrane, and we speculated that the hydrophobic tip of the β-barrel might bind within the hydrophobic substrate binding site of GroEL, inhibiting large-

scale aggregation of the PA pore and facilitating its structural analysis by electron microscopy.

Our hypothesis about the precise way in which GroEL would recognize the pore was inaccurate, but the notion that the two structures might interact to advantage proved correct. Here we show that the ATP-free substrate-binding form of GroEL interacts with heptameric forms of PA pore and that this interaction preserves the capacity of the heptamers to form fully functional pores in model membranes under conditions in which the pores would normally aggregate and become inactive. However, complex formation resulted not from an interaction of GroEL with the stem region of the mushroom-shaped pore, but rather from interaction with the globular cap, where edema factor and LF bind. We were able to view GroEL–PA pore complexes and free pores by negative-stain electron microscopy before extensive aggregation ensued, allowing us to collect more than enough individual single-particle images to generate three-dimensional reconstructions of the PA pore.

RESULTS

GroEL binds the PA prepore

Incubating GroEL with the PA prepore at pH 8.5, a condition under which the prepore-to-pore transition is not observed, gave rise to a single band that migrated above GroEL and PA prepore on native PAGE, suggesting formation of a stable complex between these two oligomers (Fig. 1a). Furthermore, adding LF to this mixture blocked formation of the GroEL–prepore complex. This blockage seemed to result from the tight binding of LF to the PA prepore (nM affinity)1, as we did not detect any interaction between LF and GroEL. Thus, binding of GroEL to the prepore may be sterically prevented by bound LF, or alternatively, LF may stabilize the prepore structure in ways that block its interaction with GroEL.

PA prepore-to-pore conversion with GroEL present

Initially, obtaining evidence for an interaction of GroEL with the PA pore proved problematic. GroEL is unstable at acidic pH, and there was little indication of GroEL binding to PA heptamers by gel electrophoresis or by negative-stain electron microscopy when we exposed mixtures of prepore and GroEL to low pH. Inducing the prepore-to-pore conversion with detergents at neutral or basic pH was also unsuccessful, as the tested detergents obscured observation of GroEL–PA pore complex formation. However, when we used a non-denaturing concentration of urea (1 M) to promote the conformational transition at neutral or mildly basic pH, the interaction between GroEL and PA heptamer pore was preserved. The efficiency and magnitude of prepore-to-pore conversion induced by 1 M urea were dependent on temperature: we observed little conversion on ice or at room temperature (22–24 °C), but a 30-s incubation at 37 °C caused efficient (80%–90%) conversion.

Under these conditions, amorphous aggregates were formed with prepore alone, and negatively stained preparations showed no other discernable structures except trapped prepore (Fig. 1b). When GroEL was present, large-scale aggregation was suppressed, and we were able to resolve structured particles, including free prepore, free GroEL, free

mushroom-shaped pore, pore–GroEL complexes and small aggregates (Fig. 1b). GroEL appeared to bind to the cap of the mushroom-shaped pores, consistent with the native gel data suggesting interaction with the face of the prepore that binds LF. The small aggregates consisted primarily of dimers, trimers and tetramers of GroEL–PA pore complexes, joined by interactions of the stems at their hydrophobic tips.

PA forms functional pores in the presence of GroEL

We tested for potential effects of GroEL on pore-forming activity of heptameric PA in planar phospholipid bilayers. We mixed GroEL and PA prepore in various molar ratios at pH 8.5 and pulsed each sample for 30 s at 37 °C in 1 M urea. We then immediately diluted samples into pH 8.5 buffer in the *cis* chamber of a planar bilayer system to a final concentration of PA pore in the chamber of <20 pM and monitored the transmembrane current as a function of time. Whereas the control sample lacking GroEL was essentially devoid of pore-forming activity, we observed strong activity in the presence of GroEL, and the activity increased with an increasing molar ratio of GroEL to PA prepore (Fig. 2a). GroEL alone did not cause a change in conductance (data not shown).

We tested whether the PA pores generated with GroEL were functional for protein translocation. We formed pores in a planar bilayer from a mixture with a 2:1 molar ratio of GroEL to PA, lowered the pH to 5.5 in both chambers and added the N-terminal fragment of LF (LF_N) to the *cis* chamber, causing nearly complete (98%) blockage of current. Raising the pH of the *trans* chamber to 7.2 induced translocation of LF_N with kinetics almost identical to that observed with pores formed in the absence of GroEL (Fig. 2b). In the absence of GroEL, it was necessary to add ~100-fold-concentrated PA pore in order to obtain a macroscopic conductance signal equivalent to that generated in the presence of GroEL (Fig. 2a). Furthermore, we normalized the kinetic traces of the LF_N translocation so that we could easily compare the two conditions. In summary, we did not find any difference in functionality between pores formed in the presence of GroEL and those formed in the absence of GroEL.

GroEL binds PA pores and is released by ATP

If GroEL interacts with the LF-binding face of the prepore (Fig. 1a) and with the cap of the PA pore (Fig. 1b), the chaperonin might also bind to PA pores in planar bilayers and affect ion conductance. We formed pores by adding prepore alone to the *cis* chamber at pH 5.5, raised the pH to 8.5 symmetrically and monitored conductance as we titrated nanomolar concentrations of GroEL into the system. The final concentration of pore in the chamber was < ~20 pM, and the largest initial concentration of GroEL used to facilitate pore insertion was ~128 pM. These low GroEL concentrations were insufficient to completely inhibit the conductance. Furthermore, simple perfusion of the *cis* chamber containing a GroEL-blocked pore resulted in a slow rise of pore conductance caused by the dissociation of bound GroEL from inserted pores due to low binding affinity (data not shown). The conductance was blocked appreciably only when additional GroEL was present at much higher concentrations. We observed a concentration-dependent blockage of current by GroEL (Fig. 2c), with a maximal inhibition of ~84%. Thus, GroEL inhibited conductance, suggesting that bound GroEL blocks access to the mouth of the pore or that it induces a closure of the

PA pore indirectly. We observed half-maximal inhibition of ion conductance by GroEL at ~144 nM, indicating a relatively weak affinity. Consistent with that observation, GroEL rapidly dissociated from pores after perfusion, whereas dissociation of LF_N was negligible under the same conditions (data not shown). In addition, we observed a rapid reversal of the GroEL-dependent conductance block ($t_{1/2}$ = ~9 s) upon adding ATP, in agreement with known functional properties of the chaperonin11 (Fig. 2d).

Classification of EM images

GroEL–PA pore complexes and free PA pore appeared solely in side-view orientations in negative-stain electron micrographs (Fig. 3). About half the GroEL was in complex with pore, and about 20% of these were individual unaggregated complexes and thus appropriate for image processing. Fewer than 1% of the GroEL–pore complexes had PA pore bound at both ends of GroEL, suggesting negative cooperativity between two rings of GroEL11, although the PA pore seemed to bind outside the central cavity. Large numbers of complexes of GroEL–PA pore particles (1,667) and free PA pore particles (1,368) were used to generate two-dimensional averages (Fig. 3, center row). The averaged GroEL–PA pore structure clearly showed GroEL binding to the cap of the pore, contradicting our initial prediction that the stem of the pore might insert into the substrate binding site of GroEL. The presence of free PA pore is consistent with a relatively weak interaction between GroEL and the PA pore, but it does not exclude the possibility that the free form represents a different conformer with a weaker affinity for GroEL. The very bright region at the tip of the pore stem is probably due to repulsion of the negative stain from the hydrophobic tip of the stem.

For the GroEL–PA pore complexes themselves, we assessed the structural variability of the interaction (see Methods). Class averages showed different degrees of tilt and off-axis shift of the PA pore relative to GroEL (Supplementary Fig. 1 online). These differences may represent true heterogeneity of the GroEL–PA pore complex due to relatively low specificity of the binding. Alternatively, the heterogeneous populations could reflect distortions due to absorption, staining, structure flattening or drying during the negative staining process. In any case, because of such heterogeneity, we masked the PA pore and GroEL moieties of the complexes and aligned them individually (Fig. 3, bottom row). The PA pore structure derived by averaging images from the pore-aligned GroEL–pore complex had a more distinct boundary density at the ends and looked more similar to free PA pore than the structure derived by alignment over the entire complex. In addition, a thin protein density that seemed to extend beyond the lower cap region was more prominent in GroEL-bound PA pore than in free PA pore (Supplementary Fig. 2 online).

Reconstruction and dimensions of the PA pore

We selected 1,368 free pore particles and 1,292 GroEL-bound PA pore particles with moderate to high correlation coefficients, classified them into 56 and 53 classes, respectively, and used the class averages for three-dimensional reconstruction. The initial reconstruction did not produce a structure with continuous density because of the very bright region at the hydrophobic tip of the stem. To compensate for the unequal distribution of the

stain around the molecules, we used a stain density ramp or gaussian spot procedure (see Methods).

We performed independent reconstructions on free PA pore and GroEL-bound PA pore with seven-fold symmetry imposed, generating 25-Å and 28-Å structures, respectively (Fig. 4 and Supplementary Fig. 3 online). The structures of free PA pore and GroEL-bound PA pore were reconstructed from an initial model of a cylinder or a sphere with radius of 80 Å, both of homogenous density (see Methods). Both reconstructions converged to indistinguishable structures, indicating that the final structures had minimal model bias. Free and GroEL-bound PA pore structures showed differences around domain 3, although the quality of the reconstruction was not sufficient to distinguish detailed structural features from noise. The free PA pore appeared to have connections between domain 3 of adjacent subunits and between domain 2 and domain 3 (Fig. 4b), whereas GroEL-bound PA pore did not have such a connection (Fig. 4a). The interior cavity of the cap region was wider in free PA pore, perhaps because of different degrees of shrinkage in stain (the presence of GroEL may alter the accessibility and accumulation characteristics of the stain). The source of these apparent differences will be resolved only when we acquire higher resolution cryo-EM images.

The dimensions of the PA pore in the GroEL-bound PA pore complex (Fig. 4a) closely matched those of a hypothetical model structure10, and the length of the PA pore stem was close to that predicted from previous biochemical analysis6. However, the stem appeared much wider in the EM structure than predicted. The widening of the stem could be due to artifacts from negative staining, the inherent flexibility of the β-barrel or both (Supplementary Discussion and Supplementary Fig. 4 online).

Truncated crystal structure prepore fit into the EM pore envelope

A comparison of the EM structures (Fig. 4) with the crystal structure of the PA prepore monomer (Fig. 5a, from PDB 1TZO (ref. 12)) indicated that domain 4 was missing from the EM structures. When we examined consecutive slices of the three-dimensional EM structure, we saw visible density areas where domain 4 was expected to be located (Supplementary Fig. 2), but these were completely excluded in the final reconstruction. Little, if any, interaction between domain 4 and domain 2 would be expected to be preserved once the β-barrel structure forms6,13. Thus, it is likely that domain 4 is too flexible in solution to be visualized by single-particle analysis.

To fit the remainder of the PA prepore with the PA pore cap structure, we removed the residues that comprised domain 4 (596–735)13 and residues that formed the β-barrel structure (275–352)6 from the atomic coordinates of the prepore crystal structure before performing manual fits with the EM structures (Fig. 5b,c). The resulting GroEL-bound PA pore EM structure fit fairly well with the prepore crystal structure in domains 1 and 3 (Fig. 5b). Domain 2, however, was constricted inward in the EM structure and extended outward in the PA prepore crystal structure, which indicates a substantial conformational change in domain 2 besides the formation of the β-barrel. By contrast, no crystal structure fit into the connections between domain 3 of neighboring subunits in the EM structure of free PA pore (Fig. 5c). In addition, the low pass–filtered surface of the PA prepore derived from the crystal structure did not match the free pore EM structure in domains 1 and 3 (Fig. 5c) as

well as it did in the GroEL-bound PA pore reconstruction. It is possible that domain 3 of the free pore structure is flexible in solution, resulting in a heterogeneous population with domain 3 in various positions (Supplementary Discussion and Supplementary Figs. 5 and 6 online).

DISCUSSION

We found that GroEL substantially inhibited aggregation during the PA prepore-to-pore transition, increasing the number of PA pores formed in model membranes. Most notably, the three-dimensional structure of these complexes was easily reconstructed using negative-stain EM, and single-particle analysis suggested that GroEL can be used to obtain higher-resolution cryostructures of the PA pore.

The data indicated that PA membrane insertion and channel formation could occur readily at pH 8.5. Thus, the low pH usually used to induce pore formation in membranes promotes the conformational change from the prepore to an insertion-competent species but does not seem to be required for the actual membrane insertion. Which molecular species in the GroEL-PA pore mixtures is (or are) responsible for forming the PA pores cannot be determined from our results. However, the specific binding between the nucleotide-free GroEL and the membrane-inserted PA pore is consistent with the notion that the structures observed by EM resemble the membrane-inserted structures.

The reconstructed PA pore structure showed a 100-Å extended region, in line with the prediction of an extended β-barrel in the pore. Biochemical evidence indicates that this extended region arises from a substantial portion of domain 2 in the prepore structure6. Our reconstructed pore complexes also indicated that domain 4 is no longer constrained in the PA pore. The position of domain 3 may also vary to some degree, at least for the free PA pore. These observations makes structural sense, as domain 4 in the PA prepore contacts the outermost residues of domain 2 proposed to form the extended β-barrel structure. The loss of this region during the transition from PA prepore to PA pore might result in the flexibilities in domains 3 and 4, in contrast to molecular dynamic simulations10 that indicated that domains 3 and 4 could form new stable interaction interfaces with the remainder of domain 2.

Our analysis showed that the PA pore stem existed in multiple orientations with respect to the cap region in the absence of lipid membranes or cell receptors. This variability could result from artifacts from negative staining, leading to a reconstructed β-barrel portion that is wider than predicted (56 Å versus ~32 Å) (Supplementary Discussion). At present, it is hard to predict if this large-scale flexibility and variability in the pore structure here would be observed in the complete receptor–pore–lipid membrane superstructure or in solution.

GroEL-facilitated insertion of membrane proteins into artificial planar bilayer systems may be a reasonable non–detergent-based method to generate homogeneous membrane protein assemblies. Both the GroEL chaperonin and the osmolyte urea provide inherent anti-aggregation and unfolding functions. The stabilization and enhanced formation of the membrane-insertable PA pore in the presence of GroEL and urea provides another example

in which a chaperonin-osmolyte folding combination has proven valuable for folding and structure determination14,15. Although the hydrophobic tip of the β-barrel remains exposed to solution in the GroEL–pore complex, the initial aggregation is substantially diminished. The decrease in aggregation could result from slower collisional rates between much larger (1,240 kDa) GroEL–pore complexes. Indeed, at higher GroEL concentrations (such as a 2:1 molar ratio of GroEL to pore oligomer), we observe very little aggregation of the GroEL–PA pore complexes by EM. Although GroEL-facilitated membrane insertion has been observed for several smaller intrinsic membrane proteins3,4,15, our work shows that GroEL increases membrane insertion for a much larger protein.

Consecutive slices of the three-dimensional PA pore structure (Supplementary Fig. 2) indicated many density regions within the PA pore, suggesting the presence of many constriction points. At this resolution, it is difficult to identify particular residues that may be involved in forming these constriction points. However, obtaining higher-resolution cryo-EM structures and modeling the changes using hybrid crystallography coupled with molecular dynamics approaches may enable us to position the functionally important phenylalanine clamp structure17. With this information, we can begin to understand the structural basis underlying the translocation mechanism of the heptameric PA pore.

In conclusion, this work indicates that GroEL is useful as a structural tool to stabilize very large–molecule complexes while preventing inappropriate aggregation. This work also demonstrates that GroEL can bind extended protein surfaces of large structures so that they can be analyzed using single-particle electron microscopy methods. We propose (i) that GroEL can be used as a general tool to increase the yields of correctly folded membrane proteins before membrane insertion and (ii) that GroEL may actually serve as a large structural scaffold to facilitate membrane protein structure determination by electron microscopy.

METHODS

Expression and purification of proteins

We overexpressed recombinant wild-type 83-kDa PA (PA_{83}) in the periplasm of *Escherichia coli* BL21 (DE3) and purified it by anion-exchange chromatography, as described18. Wild-type PA prepore was purified from trypsin-digested PA by anion-exchange chromatography19. Recombinant LF_N was expressed in the cytoplasm of *E. coli* BL21 (DE3) as an N-terminally His_6-tagged protein, purified over Ni-NTA resin and treated with bovine α-thrombin to cleave off the His tag20. Extremely pure GroEL (>99%) was provided as a gift by EdgeBiosystems based on bulk purification schemes developed earlier21.

Native gel electrophoresis of PA prepore bound to ligands

We incubated 1.5 pmol PA prepore with 1.5 pmol LF, with 3 pmol GroEL or with both LF and GroEL for 1 h on ice in 20 mM Tris buffer (pH 8.5). After the incubation, we added native-sample buffer and applied the samples directly to a 4%–12% gradient Tris-glycine gel and electrophoresed the samples at 50 V for ~3 h on ice. The resulting gel was stained

with Coomassie brillant blue overnight, destained and imaged using a Gel Logic 100 Imaging System (Kodak).

Electrophysiology

We painted22 planar lipid bilayers onto a 200-μm aperture of a 1-ml Delrin cup, using 3% (v/v) 1,2-diphytanoyl-*sn*-glycerol-3-phosphocholine in *n*-decane (Avanti Polar Lipids). *cis* (the side to which PA prepore and LF_N were added) and *trans* compartments were bathed in symmetric universal bilayer buffer containing 100 mM KCl, 1 mM EDTA and 10 mM each of potassium oxalate, phosphate and MES (pH 8.5). The membrane potential $\Delta\psi$, defined as $\Delta\psi = \psi_{cis} - \psi_{trans}$ (where $\psi_{trans} \equiv 0$ mV), was held constant throughout the experiment at +20 mV with respect to the *trans* compartment.

We initiated prepore-to-pore conversion for functional studies by incubating 0.5 μM prepore in the presence or absence of varying concentrations of GroEL (0.5–2.0 μM oligomer) in a buffer containing 20 mM Tris (pH 8.5), 150 mM NaCl and 1 M urea for 15 min on ice. We then applied a pulse of 30 s at 37 °C or 42 °C. Immediately after the pulse, 0.1 μl of the samples were added to the *cis* chamber of a lipid bilayer system, and the current was recorded continuously.

To test the treated pores for translocation activity, we added reaction mixture to the bilayer system, observing a large signal (~500 pA). The *cis* chamber was perfused with buffer using a syringe-based perfusion system (Warner Instruments) in which the rate of buffer exchange was kept constant at a flow rate of ~3 ml min^{-1} for ~3 min. Perfusion effectively removes weakly bound GroEL, free GroEL and excess PA pore from the *cis* chamber. The pH of both the *cis* and *trans* chambers was then lowered to pH 5.5 by the addition of appropriate amounts of 1 M HCl. We then added LF_N to the *cis* compartment and monitored its binding to PA pore channels by monitoring the fall in conductance (LF_N blocks the conductance through the pore before a translocation event). After perfusing the *cis* chamber to eliminate free LF_N, we initiated translocation of LF_N by increasing the pH of the *trans* chamber to pH 7.2, forming a pH gradient.

To determine the relative binding affinity of GroEL to PA pores, PA pores (~1,000 pores) were formed on the bilayer at pH 5.5, and the pH was then raised in both chambers to 8.5 before titrating GroEL into both chambers or into the *cis* chamber alone. We maintained the membrane potential at +20 mV (ref. 23).

To follow GroEL dissociation in real time, we formed ~1,000 PA pores on the membrane at pH 5.5 and then raised the pH in both chambers to 8.5. GroEL (200 nM) was added to the *cis* chamber. The conductance block by GroEL of PA pores was recorded and perfusion initiated. As excess GroEL was removed, the conductance block decreased because of the dissociation of GroEL from the PA pores. When we added ATP (5 mM) to the *cis* chamber, GroEL rapidly dissociated from the PA pores.

Sample preparation and negative-stain EM grid preparation

We prepared solution containing 0.5 μM GroEL and 0.5 μM PA prepore or 0.5 μM PA prepore solution in buffer containing 1 M urea, 50 mM Tris, 50 mM KCl and 10 mM

$MgCl_2$, pH 7.5, on ice. GroEL–PA prepore solution was incubated at 37 °C for 30 s. Samples were diluted either four-fold or two-fold (for GroEL–PA solution or PA solution, respectively) with buffer containing 50 mM Tris, 50 mM KCl and 10 mM $MgCl_2$, pH 7.5. For EM grid preparations, this diluted mixture was applied onto carbon-coated Cu300 EM mesh grids and stained with 2% uranyl acetate.

Electron microscopy and two-dimensional image analysis

We recorded images using a minimal-dose protocol at a magnification of 60,000 with a JEOL 1200EX electron microscope at a defocus of 0.67 μm and digitized them with a Microtek ScanMaker i900 scanner at a pixel size of 3.53 Å on the specimen. Image analysis was performed with SPIDER24. We selected 1,778 GroEL–pore particles and 1,407 free PA pore particles from 89 micrographs and aligned them by reference-free procedures. We applied masks to GroEL–PA pore particles, leaving only the GroEL or PA pore section of the complex after the initial alignment with the entire GroEL–PA pore complex, and repeated the alignment procedure with the masked particles to produce separate averages of the GroEL portion and the PA pore section of the complex. We generated two-dimensional averages of free PA pore, GroEL–PA pore complex and GroEL-bound PA pore from 1,368, 1,667 and 1,292 particles, respectively. GroEL–PA pore particles that were aligned with a mask around GroEL were classified based on PA pore region, using multivariate statistical analysis to demonstrate the variable positioning of the bound pore.

Three-dimensional reconstruction and structure analysis

Aligned particles of free pore and GroEL-bound pore were classified into 56, 53 and 73 classes by multivariate statistical analysis and hierarchical classification of the GroEL-pore particles, based on either the pore or GroEL. To account for the low accumulation of the stain along the hydrophobic stem, we superimposed a negative circular density (gaussian distribution with a σ^2 of 50 Å with the center at the tip of the stem) or a ramp of density on the upper half of the pictures above the base of the stem to each class average. Class averages were masked before three-dimensional reconstructions. Initial models for the reconstruction were a cylinder (radius = 35 Å, height = 165 Å) or a sphere (radius = 80 Å) for the PA pore. Three-dimensional structures were reconstructed by iterations of eulerian angle assignment to the class averages by projection matching from the model structure and construction of a new model with newly assigned eulerian angles. All reconstructions were low-pass filtered at 20 Å. Resolution of the reconstructions was determined by Fourier shell correlation between two reconstructions created from odd-numbered particles and even-numbered particles at a value of 0.5. All surface representations were adjusted to a threshold of 100% volume of the proteins. Fitting of the crystal structure of heptameric PA prepore (PDB 1TZO) into the EM structures was done manually with Chimera25. Residues 275–352 from domain 2 are thought to unfold from the PA prepore structure to form a β-barrel. These residues, as well as the entire domain 4 (596–735), were deleted from the PDB file before fitting.

Note

Refer to Web version on PubMed Central for supplementary material.

Acknowledgments

M.T.F. dedicates this work to the memory of Earl R. Stadtman, his mentor during his postdoctoral years at the US National Institutes of Health (NIH). Earl's influence, scientific philosophy and sense of generosity will be with M.T.F. for the rest of his days. This research was supported in part by US National Science Foundation (NSF) grant MCB-0445936 (M.T.F.), NIH grant R41 GM080074 (M.T.F.), a grant from the Kansas Technology Enterprise Corporation (M.T.F.) and NIH grant 5R37AI022021 (R.J.C.). The NSF grant supported J.J. and M.B. GroEL was a gift from EdgeBiosystems.

References

1. Young JA, Collier RJ. Anthrax toxin: receptor binding, internalization, pore formation, and translocation. Annu Rev Biochem. 2007; 76:243–265. [PubMed: 17335404]
2. Krantz BA, Finkelstein A, Collier RJ. Protein translocation through the anthrax toxin transmembrane pore is driven by a proton gradient. J Mol Biol. 2006; 355:968–979. [PubMed: 16343527]
3. Deaton J, et al. Functional bacteriorhodopsin is efficiently solubilized and delivered to membranes by the chaperonin GroEL. Proc Natl Acad Sci USA. 2004; 101:2281–2286. [PubMed: 14983001]
4. Sun J, et al. Asymmetric binding of membrane proteins to GroEL. Arch Biochem Biophys. 2005; 434:352–357. [PubMed: 15639236]
5. Benson EL, Huynh PD, Finkelstein A, Collier RJ. Identification of residues lining the anthrax protective antigen channel. Biochemistry. 1998; 37:3941–3948. [PubMed: 9521715]
6. Nassi S, Collier RJ, Finkelstein A. PA63 channel of anthrax toxin: an extended beta-barrel. Biochemistry. 2002; 41:1445–1450. [PubMed: 11814336]
7. Petosa C, Collier RJ, Klimpel KR, Leppla SH, Liddington RC. Crystal structure of the anthrax toxin protective antigen. Nature. 1997; 385:833–838. [PubMed: 9039918]
8. Lacy DB, et al. A model of anthrax toxin lethal factor bound to protective antigen. Proc Natl Acad Sci USA. 2005; 102:16409–16414. [PubMed: 16251269]
9. Song L, et al. Structure of staphylococcal alpha-hemolysin, a heptameric transmembrane pore. Science. 1996; 274:1859–1866. [PubMed: 8943190]
10. Nguyen TL. Three-dimensional model of the pore form of anthrax protective antigen. Structure and biological implications. J Biomol Struct Dyn. 2004; 22:253–265. [PubMed: 15473701]
11. Horovitz A, Fridmann Y, Kafri G, Yifrach O. Review: allostery in chaperonins. J Struct Biol. 2001; 135:104–114. [PubMed: 11580260]
12. Lacy DB, et al. Structure of heptameric protective bound to an anthrax toxin receptor: a role for receptor in pH-dependent pore formation. Proc Natl Acad Sci USA. 2004; 101:13147–13151. [PubMed: 15326297]
13. Rosovitz MJ, et al. Alanine-scanning mutations in domain 4 of anthrax toxin protective antigen reveal residues important for binding to the cellular receptor and to a neutralizing monoclonal antibody. J Biol Chem. 2003; 278:30936–30944. [PubMed: 12771151]
14. Voziyan PA, Jadhav L, Fisher MT. Refolding a glutamine synthetase truncation mutant in vitro: identifying superior conditions using a combination of chaperonins and osmolytes. J Pharm Sci. 2000; 89:1036–1045. [PubMed: 10906727]
15. Voziyan PA, Johnston M, Chao A, Bomhoff G, Fisher MT. Designing a high throughput refolding array using a combination of the GroEL chaperonin and osmolytes. J Struct Funct Genomics. 2005; 6:183–188. [PubMed: 16211517]
16. Goulhen F, Dé E, Pagès JM, Bolla JM. Functional refolding of the *Campylobacter jejuni* MOMP (major outer membrane protein) porin by GroEL from the same species. Biochem J. 2004; 378:851–856. [PubMed: 14662009]
17. Krantz BA, et al. A phenylalanine clamp catalyzes protein translocation through the anthrax toxin pore. Science. 2005; 309:777–781. [PubMed: 16051798]
18. Miller CJ, Elliott JL, Collier RJ. Anthrax protective antigen: prepore-to-pore conversion. Biochemistry. 1999; 38:10432–10441. [PubMed: 10441138]

19. Wigelsworth DJ, et al. Binding stoichiometry and kinetics of the interaction of a human anthrax toxin receptor, CMG2, with protective antigen. J Biol Chem. 2004; 279:23349–23356. [PubMed: 15044490]

20. Zhang S, Finkelstein A, Collier RJ. Evidence that translocation of anthrax toxin's lethal factor is initiated by entry of its N terminus into the protective antigen channel. Proc Natl Acad Sci USA. 2004; 101:16756–16761. [PubMed: 15548616]

21. Voziyan PA, Fisher MT. GroE-mediated folding of glutamine synthetase under non-permissive conditions; off-pathway aggregation propensity does not determine the co-chaperonin requirement. Protein Sci. 2000; 9:2405–2415. [PubMed: 11206062]

22. Mueller P, Rudin DO. Induced excitability in reconstituted cell membrane structure. J Theor Biol. 1963; 4:268–280. [PubMed: 5875200]

23. Blaustein RO, Finkelstein A. Voltage-dependent block of anthrax toxin channels in planar phospholipid bilayer membranes by symmetric tetraalkylammonium ions. J Gen Physiol. 1990; 96:905–919. [PubMed: 1704045]

24. Frank J, et al. SPIDER and WEB: processing and visualization of images in 3D electron microscopy and other fields. J Struct Biol. 1996; 116:190–199. [PubMed: 8742743]

25. Huang CC, Couch GS, Pettersen EF, Ferrin TE. Chimera: an extensible molecular modeling application constructed using standard components. Pac Symp Biocomput. 1996; 724

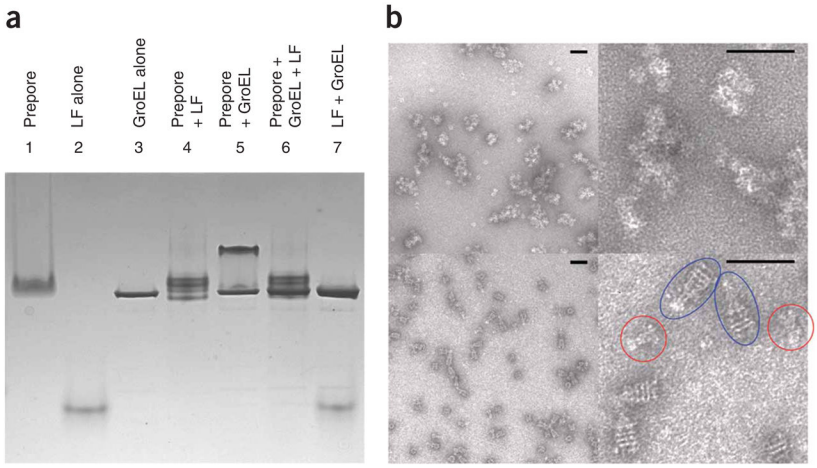

Figure 1.

GroEL binds to the PA prepore and pore. (**a**) Native PAGE, using 1.5 pmol of each protein, stained with Coomassie blue. The four discrete bands seen in lane 4 presumably represent (from bottom to top) uncomplexed PA prepore and prepore in complex with one, two or three molecules, respectively, of LF. (**b**) GroEL prevents large-scale aggregation of PA pores. Upper left, negative-stain EM image of PA pore after 37 °C incubation for 30 s in pH 7.5 buffer with 1 M urea. Aggregated particles and free PA prepore can be seen. Upper right, higher-magnification view of image at upper left. No conserved structure can be recognized in the aggregates, except the prepore. Lower left, pore and GroEL after 37 °C incubation for 30 s in pH 7.5 buffer with 1 M urea. Free PA pore, GroEL–PA pore complexes and aggregated PA pore and GroEL–PA pore complexes can be seen. Lower right, higher-magnification view of image at lower left. Free pores are circled in red, pore–GroEL complexes in blue. Aggregation in the lower left panel shows characteristic tip-to-tip interaction. Scale bars, 400 Å.

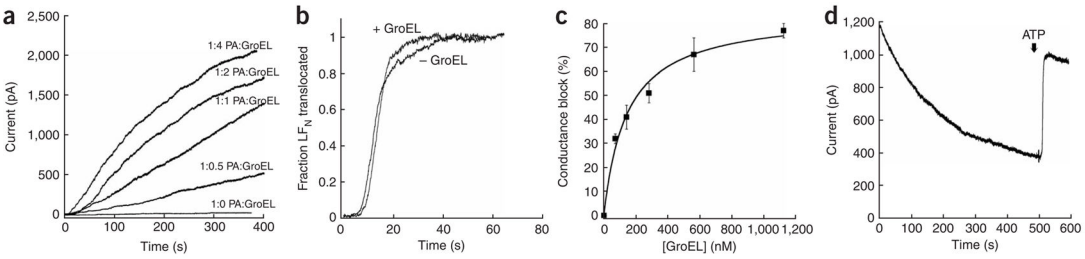

Figure 2.

PA pore formed in the presence of GroEL is functional. (**a**) GroEL preserves pore-forming potential of prepore. Macroscopic current records of PA pores formed by addition of urea (final concentration 1 M) to prepore in the presence of various amounts of GroEL. (**b**) PA pores formed in the presence of GroEL translocate LF_N. Vertical axis, the fraction LF_N translocated through PA pores formed in the presence or absence of GroEL. The half-time of translocation for GroEL-containing PA samples ($t_{1/2}$ = 11 s) was similar to that observed with wild-type PA ($t_{1/2}$ = 8 s). (**c**) GroEL binds to PA pores preformed in planar lipid bilayers. Average of three experiments, with s.e.m. GroEL was titrated into both compartments of the bilayer apparatus, but similar results were obtained when GroEL was titrated into the *cis* compartment alone. (**d**) Addition of ATP to PA pores blocked by GroEL results in rapid GroEL release. The plot is a representative macroscopic current trace showing the blockage of PA pores by 200 nM GroEL and the resulting disappearance of that blockage upon addition of ATP (final concentration 5 mM).

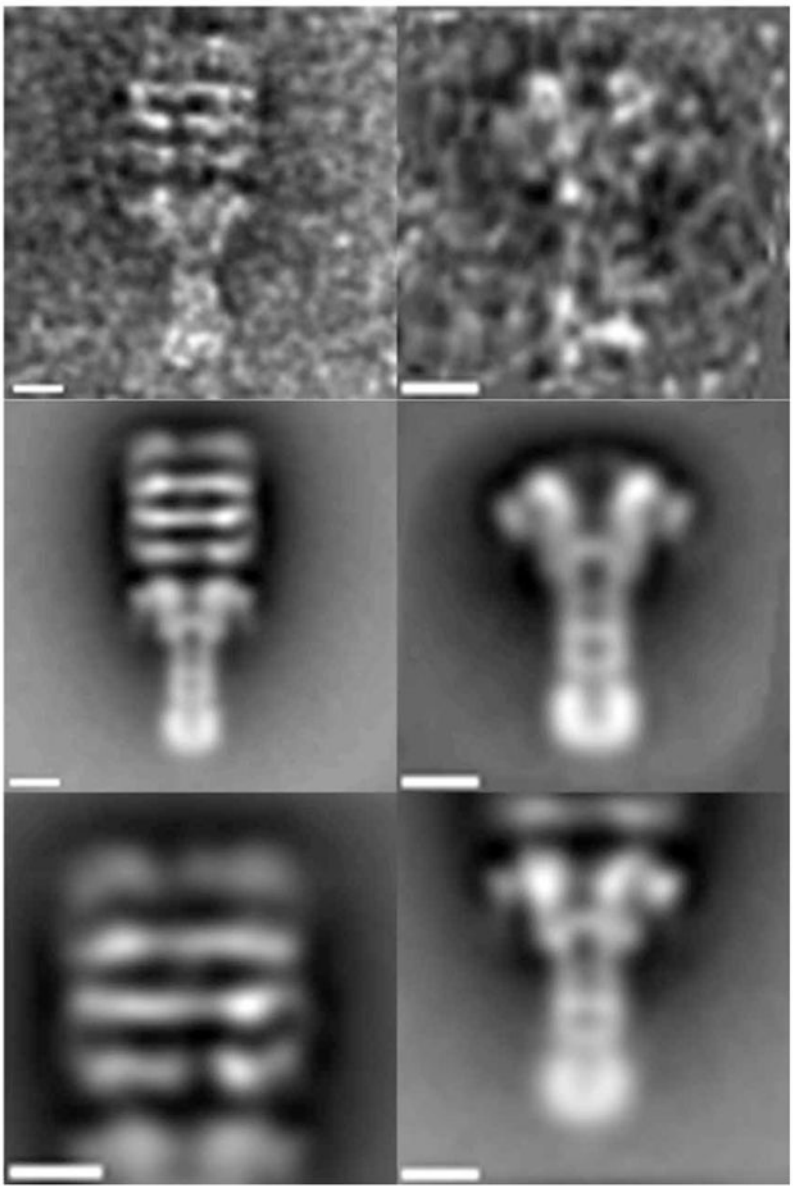

Figure 3.

Two-dimensional average of GroEL-bound and free PA pore particles. Top row, left: representative EM image of a single PA pore–GroEL complex. Top row, right: representative EM image of a single free PA pore. Middle row, left: average of 1,667 PA pore–GroEL complexes. Middle row, right: average of 1,368 free PA pore particles. Bottom row, left: average of GroEL from the PA pore–GroEL complex aligned using only the GroEL portion. Bottom row, right: average of PA pore from the PA pore–GroEL complex aligned using the PA portion. Scale bars, 50 Å.

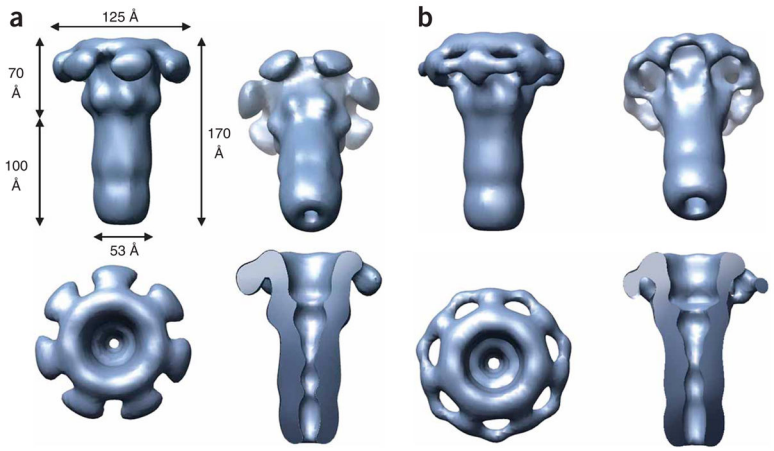

Figure 4.

Three-dimensional reconstructions of GroEL-bound and free PA pore particles. (**a**) Three-dimensional reconstructions of GroEL-bound pore. Top left, side view of GroEL-bound pore. Top right, 45° tilt of GroEL-bound pore. Bottom left: end view of GroEL-bound pore from the cap. Bottom right, half view of GroEL-bound pore. (**b**) Three-dimensional reconstructions of free pore. Top left, side view of free pore. Top right, 45° tilt of free pore. Bottom left, end view of free pore from cap region. Bottom right, half view of free pore.

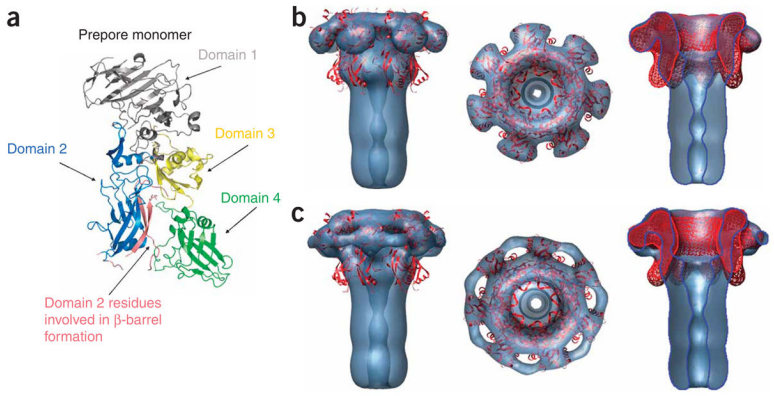

Figure 5.

Manual fit of the PA prepore crystal structure into the PA pore EM structure. (**a**) Crystal structure of the 63-kDa PA (PA_{63}) prepore monomer (PDB 1TZO) with labeled domains. (**b**) The crystal structure of the PA prepore was fit into the GroEL-bound PA pore EM structure. Domain 4 and residues 275–352 were removed from the PDB file. Domains 1 and 3 fit well, whereas the crystal structure of domain 2 extended outward from the pore structure. Left, side view. Middle, view from cap end. Right, half view of the fit. The crystal structure was low-pass filtered to 20-Å resolution. (**c**) The crystal structure of the prepore was fit into free PA pore EM structure. No crystal structure–derived mass fits into the connections between domain 3 of EM structure. Left, side view. Middle, view from cap end. Right, half view of the fit. The crystal structure was low-pass filtered to 20-Å resolution.